

# Framework for 3D data modeling and Web visualization of underground caves using open source tools

Ivo Silvestre<sup>1</sup>, José I. Rodrigues<sup>1,2</sup>, Mauro Figueiredo<sup>1,2</sup>, Cristina Veiga-Pires<sup>1,3</sup>

<sup>1</sup>Centro de Investigação Marinha e Ambiental – CIMA

<sup>2</sup>Instituto Superior de Engenharia – Universidade do Algarve

<sup>3</sup>Faculdade de Ciências e Tecnologia – Universidade do Algarve \*

## Abstract

Terrestrial Laser Scanning is a very useful technique for cave studies. This surveying method creates point clouds with high detail levels for 3D model generation, which is indeed useful for either reconstruction, geomorphological studies or virtual visits of caves. The present work generated a 3D model of a cave chamber and developed a framework for 3D data visualization on the Web.

Identifying geomorphological structures is one of the goals of this project. The generated 3D-mesh represents the surface model of the cave chamber, which is important to study its geomorphological features. A topological structure of the 3D-mesh was implemented to get an efficient algorithm to help determining stalactites. The recognition and positioning of cave stalactites can provide information on hidden cave features responsible for cave geomorphology.

The possibility to publish 3D data on the Web is of particular interest for the geospatial field. For this reason, it was decided to make the cave model available in the Web by developing a 3D graphical interface where users can navigate and interact with the three-dimensional models of the cave. For this Web framework, X3D, WebGL and X3DOM were used. Such solution does not require any additional plug-ins or components.

**Keywords:** Cave surveying, Terrestrial Laser Scanning (TLS), 3D-mesh, MeshLab, X3D, X3DOM

## 1 Introduction

The present work is part of the project SIPCLIP<sup>1</sup>. In the context of the global warming, SIPCLIP project aims to provide information on past regional climates, to better constrain their complex interactions with global climate and acquire new information to document past climatic conditions in the South-western Iberian Peninsula. This information is based on the analysis of cave speleothems, which are useful records for paleoclimatic reconstruction.

To analyze speleothems a Terrestrial Laser Scan survey of a karst cave was done. The selected cave is located in the southernmost

\* {imsilvestre,jirodrig,mfiguei,cvpires}@ualg.pt

<sup>1</sup>PTDC/AAC-CLI/100916/2008 – Temperature, precipitation regime and soil conditions in Southwestern Iberian Peninsula under a warmer climate - Insight from the past

Permission to make digital or hard copies of part or all of this work for personal or classroom use is granted without fee provided that copies are not made or distributed for commercial advantage and that copies bear this notice and the full citation on the first page. Copyrights for components of this work owned by others than ACM must be honored. Abstracting with credit is permitted. To copy otherwise, to republish, to post on servers, or to redistribute to lists, requires prior specific permission and/or a fee. Request permissions from [permissions@acm.org](mailto:permissions@acm.org).  
Web3D 2013, June 20 – 22, 2013, San Sebastian, Spain.  
Copyright © ACM 978-1-4503-2133-4/13/06 \$15.00

region of Portugal (Algarve) [Silvestre et al. 2012].

This paper describes an approach for the conception of a 3D model from the laser scan data collection that enables the identification and mapping of geomorphological structures inside a cave. In this way, a framework was developed for the 3D data modeling and Web visualization.

The Section 2 presents the process of scanning of the cave chambers with high level of data density. It is also described the process of data acquisition which was a very complex task due to the difficult accesses and the working environment. Chambers have a lot of irregular surfaces. The obtained point cloud from laser scan has about 45 million points to assure high level of detail.

Identifying geomorphological structures is one of the goals of this research project. Point clouds by themselves do not provide enough information about the cave chamber surface. Section 3 presents approached for generating a 3D-mesh from the point cloud using an open source tool.

The surface model of the cave is important to study its geomorphological features. In the Section 4 we develop algorithms for the recognition and positioning of cave stalactites that can provide information on hidden cave features responsible for cave geomorphology. We also implemented a topological structure for the 3D-mesh to get an efficient algorithm to help determining stalactites.

The advances in computer hardware and Internet connection speed makes possible the visualization of 3D models in the Web. This is of particular interest for the geospatial research. Section 5 presents our approach to provide a 3D graphical interface where users can navigate and interact with the three-dimensional model of a cave. We developed a Web3D site for the visualization of a cave chamber using X3D, WebGL and X3DOM, that runs on Firefox, Google Chrome, Safari and Opera web browsers without plug-ins.

## 2 Terrestrial Laser Scanning survey

The selected cave, known by the local speleologists as *Algar do Penico*, is located in the southernmost region of Portugal (Algarve), to the west of the city of Loulé (see Figure 1). This cave has an extension of about 80 meters, a gap of 14 meters and a depth of approximately 20 meters. It is composed by two chambers connected by a vertical narrow gallery of about 5 meters.

In the context of this project and with the objective of mapping the cave and its geomorphological structures for environmental and geological studies, it was decided to survey its interior chambers. Each chamber was surveyed independently due to its morphological characteristics. The work presented in this paper is focused in the main chamber. In order to survey the cave with high levels of data density for close range applications a laser scanner was used. The process of data acquisition in the interior of the cave was a very complex task due to the difficult accesses and the working environment, which has a lot of irregular surfaces.



**Figure 1:** Algar do Penico cave location in the southernmost region of Portugal (Algarve).

Terrestrial Laser Scanning is a relatively new technology that offers high resolution surveys. The scanner's pulsed laser ranging device, coupled with beam deflection mechanisms, facilitates rapid acquisition of a huge number of three-dimensional point measurements. One of the great advantage of this surveying method is the high-resolution surface geometry that permits accurate and detailed surface reconstruction and modeling as well as superior visualization relative to existing measurement technologies [Roncat et al. 2011].

The main chamber of the cave Algar do Penico was surveyed with a Terrestrial Laser Scanner (TLS), more specifically, the *Leica ScanStation C10* laser scanner system mounted on a tripod. The specifications of this unit include a  $360^\circ$  horizontal field of view and a maximum of  $270^\circ$  vertical field of view. The scanner emits pulses of green laser light that sweeps across the chamber surfaces and sends back measurements with precise  $x$ ,  $y$  and  $z$  coordinates, each having an associated intensity value and color. The scanner enables point cloud to be captured that correspond to true point positions where the laser pulse hits the object. The point cloud represents the shape and position of scanned surfaces relative to the position of the scanner. In the present paper we call *station* each location where the unit is positioned to scan a point cloud data.

The shape of the chamber has a lot of irregular surfaces and some of them can not be seen from the laser scan unit in one single location. Thus, multiple stations are required to avoid gaps in point clouds due to hidden surfaces. Due to the shape of the chosen chamber three stations were used. Positioning these stations is a critical task to assure the maximum cover of the chamber cavity and to reduce gaps in the final point cloud data collection.

The 3D laser scanner point cloud data was collected with a *point spacing* of 20 seconds of arc. Distance between closest points may vary according distance from station. Due to the dimensions of the cave chamber the maximum distance between closest points is less than one centimeter.

Considering cave chamber dimensions, the adopted resolution and the number of stations, three point cloud data sets were obtained with about  $15 \times 10^6$  points each. Raw data includes seven values,  $x$ ,  $y$  and  $z$  coordinates, intensity ( $i$ ), and three colors of RGB for each point. Thus, a total of  $45 \times 10^6$  point raw data arrays with seven values was obtained.

As mentioned above, coordinates of points scanned from different stations are in different local coordinate systems. Thus a registration process must be applied. Registration is a process that aligns individual point clouds into a single Cartesian reference datum. It is enabled through the use of artificial targets that were scanned during the survey [Tsakiri et al. 2007].

Six registration targets were placed inside the chamber in order to have at least three tie points to register each local scanner locations into a single point cloud representing the chamber. In Table 1 we can identify that there are four common targets surveyed from station St01 and station St02 (tg01, tg02, tg05 and tg06). The same occurs for the station St01 and St03 (tg01, tg03, tg04 and tg05).

The registration process involves coordinate transformations using mathematical affine transformations in three-dimensional space. This process of the scans for st02 and st03 was done with a root mean square error of about 25mm and 11mm, respectively.

Used targets are 6" circular planar with two concentric circles. They are designed to allow easy identification and extraction [Barbarella and Fiani 2012].

Surveyed points on targets present a well differentiated intensity  $i$  concerning whole chamber surface. Table 1 presents the average intensity for target point data for each target. Only points inside a blue disk sector between 2 and 6 inch radius were considered. Its values vary between 1850 and 1933 and the corresponding root mean square error is less than 21.

Small values of intensity presented in Table 1 were observed for targets tg01 and tg03 surveyed from station st03. For the same targets, a low number of collected points (# points) is also pointed. Both facts motivate us to a more detailed study on precision about targets.

**Table 1:** Statistics for the surveyed targets inside the chamber.

St	Tg	$\bar{i}$	$\sigma_i$	# points
01	01	1898	17	7835
	02	1880	17	8343
	03	1912	21	7067
	04	1932	19	8692
	05	1902	20	8301
	06	1913	24	8860
02	01	1917	18	9539
	02	1875	16	7222
	05	1896	19	7652
	06	1914	22	8945
03	01	1860	14	2549
	03	1852	11	1468
	04	1933	20	9591
	05	1870	16	5052

As mentioned before, targets are planar circular devices. Thus, all their scanned points lie on a single plane and the collected coordinates should satisfy the equation of this plane.

A plane equation is of the form

$$Ax + By + Cz = D,$$

where  $(x, y, z)$  are the coordinates of any its points and  $A$ ,  $B$ ,  $C$  and  $D$  constant coefficients. The center point of the station does not lie on this plane. Thus,  $D \neq 0$  and the previous plane equations can be simplified

$$A'x + B'y + C'z = 1.$$

The system of equations for all points of each target can be expressed as a matrix equation:

$$Kw = u + \varepsilon \quad (1)$$

where  $K$  is the  $m \times 3$  matrix,  $w$  the vector of plane coefficients,  $u$

the  $m$  column vector of 1's and  $\varepsilon$  the  $m$  vector of residuals:

$$K = \begin{bmatrix} x_1 & y_1 & z_1 \\ x_2 & y_2 & z_2 \\ \vdots & \vdots & \vdots \\ x_n & y_n & z_n \end{bmatrix}, \quad w = \begin{bmatrix} A' \\ B' \\ C' \end{bmatrix}$$

$$u = [1 \ 1 \ \dots \ 1]^T \text{ and } \varepsilon = [\varepsilon_1 \ \varepsilon_2 \ \dots \ \varepsilon_m]^T.$$

Solving the equation 1 using least square adjustments to estimate plane coefficients  $\bar{w}$ ,

$$\bar{w} = (K^T K)^{-1} K^T u$$

The residuals values  $\varepsilon_i$  correspond to the distance between each point data and the average plane and can be estimated from equation 1,  $\varepsilon = K\bar{w} - u$ . The mean squared error of residuals  $MSE = (\varepsilon^T \varepsilon) \frac{1}{n}$  was computed and the root mean square error, RMSE is presented in Table 2. Globally, RMSE is less or equal to 1mm. This fact reveals the very high-precision of coordinates.

Let  $\vec{N}$  be a vector perpendicular to the plane of target and  $\vec{ST}$  the position vector of the center of the target. When laser light ray that hits the center of the target is perpendicular to the plane of the target, vectors  $\vec{N}$  and  $\vec{ST}$  are collinear. Computed angles  $\alpha$  between vector  $\vec{N}$  and  $\vec{ST}$  are presented in Table 2 for each target. This angle is 0 when  $\vec{ST}$  is orthogonal to the target plane (and collinear with  $\vec{N}$ ).

**Table 2:** Targets precision measurements, and distance and orientation between stations and targets.

St	Tg	RMSE (mm)	$d(St, Tg)$ (m)	$\alpha$ (deg)
01	01	0.8	2,621	34,2733
	02	0.5	4,256	16,6815
	03	0.4	6,828	42,5264
	04	0.3	9,252	15,5800
	05	0.3	6,727	20,4409
	06	0.4	5,744	23,0697
02	01	0.5	4,5860	11,3771
	02	0.3	6,7333	28,6347
	05	0.5	4,1489	30,2960
	06	0.7	3,4935	22,6567
03	01	0.3	6,1118	54,3545
	03	0.7	2,8984	64,8606
	04	1.0	2,7055	13,2730
	05	0.2	8,8087	51,4625

High values of  $\alpha$  shown in Table 2 were observed from station st03 to targets tg01 and tg03. This fact allows us explaining the low number of collected points for each target. High values of the angle reduce the number of hitting light rays which have increments of  $20^\circ$ . The average intensity values does not seems to be affected by the angle between light rays except when  $\alpha$  is greater than  $45^\circ$ . However, this fact must be confirmed in future work because of the importance of understanding the characteristics of the intensity data parameter.

Besides the angle, intensity values are affected by surface material [Voegtle et al. 2008].

### 3 3D-mesh generation

A point cloud with about 45 million points was obtained from laser scan surveys as described in the previous section. Identifying geomorphological structures is one of the goals of this research

project. Point cloud do not provide enough information about the cave chamber surface. For this reason it is necessary to generate a surface model.

Computational representation of surfaces is a widely studied problem, with a vast bibliography of reference. Surfaces are usually represented by a collection of vertices, edges and faces, known as a *polygonal mesh* or *polygonal soup*, defining the shape of a polyhedral object. The faces of the mesh usually consist of triangles or quadrilaterals, where each face corresponds to a set of three vertices or four vertices, respectively [Tobler and Maierhofer 2006]. In the present work, a triangular 3D-mesh was adopted.

We used the *Meshlab* software [Cignoni et al. 2008] for the 3D-mesh generation of the cave chamber. MeshLab<sup>2</sup> is a free and open source software for mesh processing and editing. Furthermore, it works with a huge number of common 3D file formats, such as, PLY, STL, OBJ, 3DS, COLLADA, PTX, PTS, XYZ, ASC, X3D and VRML. There are several algorithms to do the surface reconstruction from point clouds. MeshLab has several methods for surface reconstruction. We explored a ball pivoting variant and Poisson's reconstruction.

*Ball-Pivoting Algorithm* (BPA) computes a triangle mesh interpolating a given point cloud. It uses a ball of fixed radius  $r$  that traverses the point cloud by pivoting front edges and attaching triangles to the mesh [Bernardini et al. 1999]. In the present case, this algorithm resulted in a mesh with a large number of face gaps. This is associated to the input point cloud that has holes. This problem may occur on laser scans surveys due to problems with visibility or with optical properties of the surface [Chalmoviansky and Juttler 2003]. One of the ways to reduce these holes is to increase the number of stations of the laser scan during the survey, but due to the physical characteristics of the cave cavity such solution can be very difficult to implement (or maybe impossible). This was one of the reasons to choose the *Poisson Surface Reconstruction* method for 3D-mesh generating in our case study.

Unlike the Ball-Pivoting Algorithm, *Poisson Surface Reconstruction* needs oriented vertex normals for its input data. These normals can be computed as a normalized average of the surface normals to the faces containing that vertex [Glassner 1994]. The vertex normals allow to determine the faces orientations. In this particular case, the faces may be oriented to the interior or the exterior of the cave chamber.

The Poisson Surface Reconstruction is based on the observation that the normal field of the boundary of a solid can be interpreted as the gradient of the solid's indicator function. Therefore, given a set of oriented points sampling the boundary of a solid, a 3D-mesh can be obtained by transforming the oriented point samples into a continuous vector field in 3D. This is performed finding a scalar function whose gradients best match the vector field, and extracting the appropriate isosurface [Kazhdan et al. 2006]. Although a thorough analysis of this algorithm is beyond the scope of this paper, it is useful to note that the vertices of the faces of these meshes do not coincide with the points of the survey. The Poisson Surface Reconstruction method estimates a surface more visually pleasant and more realistic than Ball-Pivoting Algorithm surface result.

The surface obtained with Poisson Surface Reconstruction has a variable detail level depending on the input parameter of the *octree depth*. The octree depth parameter is the maximum depth of the tree that will be used for the surface reconstruction. Increasing the depth, the surface gets more details. The number of faces and vertices also increases as it is shown in Table 3. This table presents the number of vertices, faces and the file size for several 3D-meshes

<sup>2</sup><http://meshlab.sourceforge.net/>

generated with octree depths of 10, 11, 12 and 13. Three dimensional meshes are stored in PLY file format. High values of octree depth increase the amount of data from 100MB to 2.4GB.

**Table 3:** 3D-meshes generated from Poisson Surface Reconstruction with octree depths of 10, 11, 12 and 13.

depth	# vertices	# faces	size (MB)
10	1316365	2630424	99
11	5016981	10030156	396
12	15628234	31252894	1300
13	28272558	56541528	2400

A compromise has to be achieved between the complexity of the 3D-mesh, the realistic visualization of the chamber, and real time interaction. For these reasons, we used the Poisson Surface Reconstruction method with an octree depth of 11 to generate a 3D-mesh with about 5 million vertices and 10 million faces. This method returned a closed surface even where the point cloud is more sparse. Figure 2 shows the 3D-mesh of the cave chamber, where we can navigate in real time, in a desktop computer with an Intel Core i7 3.40GHz, 8GB of memory RAM and a NVIDIA Quadro 4000 graphic card (with 2GB of dedicated memory) using MeshLab. The operating system is the 64-bit Ubuntu 12.04 LTS.

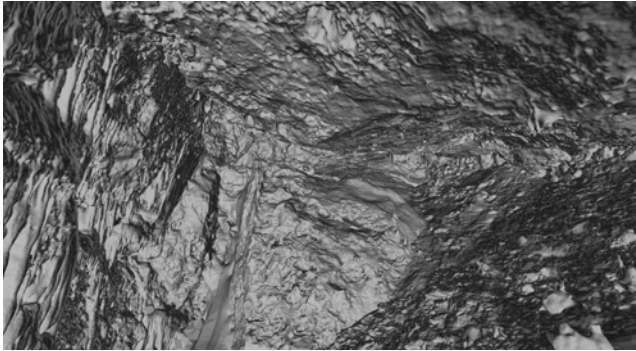


**Figure 2:** Example of the cave chamber 3D-mesh obtained with Poisson Surface Reconstruction with a depth of 11.

## 4 Identification of geomorphological structures from 3D-mesh

The speleogenetic studies aimed deciphering the origin of caves and details of specific processes which led to the existing cave structures, by studying cave morphology and its meso- and micro-morphological features. These smaller-scale features are typically not represented on the standard cave map obtained, for example, by electronic distance measurements [Roncat et al. 2011].

Accordingly, one of the main objectives of this work is to identify and map the geomorphological structures existent inside the cave Algar do Penico.

### 4.1 Geomorphological structures

The studied cave system is a relict cave in the sense that no running stream is present nowadays. Therefore the cavities, chambers and galleries, in this system, are dominated by breakdowns, and deposition of sediment and speleothems. Speleothems are cave mineral deposits, usually formed of calcite whose precipitation processes are mainly related to carbon dioxide levels in the cave percolation water. Stalactites are speleothems hanging from the cave roof that

form where percolation water seeps, mainly along geomorphological features in the cave ceiling such as faults or diaclasses that represent preferential plans for water dripping. The recognition and positioning of cave stalactites can therefore give some information on major hidden cave features responsible for cave geomorphology. Stalagmites are speleothems that grow upward from the cave floor. They are therefore the complement of stalactites. Accordingly, these specific cave structures may also give clues on important delineation and alignments influencing the cave geomorphology [Ford and Williams 2007].

### 4.2 Graphs and adjacencies

The polygon mesh previously referred (see Section 3) can be also called polygon soup. A polygon soup is a mesh that consists of a collection of triangles with no particular ordering and without any kind of topological information associated. This type of structures are the default output format when geometry is exported from a 3D modeling software such as MeshLab, Blender or Maya [Shen et al. 2004].

A graph consists of a finite set of vertices,  $V$ , and a set of edges,  $E$ , where each  $e \in E$  is a pair of vertices. Given an edge,  $e = \{u, v\}$ , vertices  $u, v \in V$  are *adjacents*. A *path* is a sequence of pairwise adjacent vertices without repetition of any vertex except possibly the first and the last which can be the same. When the first and the last vertices of a path are the same, the *closed path* is also called a *cycle*. Graphs are often sketched as node-link diagrams in which the vertices are represented as points and the edges as lines. When a graph draw can be embedded in the plane with no edge crossing except at their common vertices the graph is called *planar*. Let  $G = (V, E)$  be a plane graph. The plane regions bounded by the edges of  $G$  are called faces.

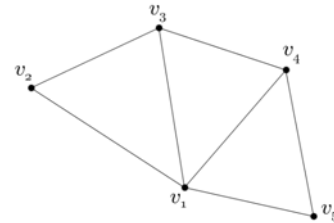


**Figure 3:** Planar graph with 5 vertices and 7 edges.

Figure 3 presents a planar graph  $G$  with 5 vertices and 7 edges and 4 faces (3 triangles and the exterior face). Vertex  $v_1$  is adjacent to all other vertices,  $\{v_3, v_4\}$  is an edge of  $G$ ,  $\{v_1, v_2, v_3, v_4\}$  is a path and  $\{v_1, v_2, v_3, v_1\}$  is a face.

There are several data structures to store graphs. For computational purposes, we adopt the adjacency list data structure where for each vertex correspond the list of adjacent vertices.

For the graph in Figure 3, the adjacency list is as follows:

$$Adj = \{v_1 : [v_2, v_3, v_4, v_5], v_2 : [v_1, v_3] \quad (2)$$

$$v_3 : [v_1, v_2, v_4], v_4 : [v_1, v_3, v_5], v_5 : [v_1, v_4]\}$$

From a 3D-mesh polygonal soup a definition of a graph  $G = (V, E)$  is a straight process. The vertices set  $V$  is the vertices set of the mesh and edges of  $G$  are the edges of the mesh. The advantage

of the graph structure is that it includes explicit topological information which allows the implementation of an efficient algorithm to determine local minima in the mesh (see Algorithm 1).

The information of vertex adjacencies was organized with the help of Python<sup>3</sup> dictionaries. These data types are sometimes found in other languages as associative arrays or hash tables. A Python dictionary is an unordered collection of key-value pairs, with the requirement that the keys are unique. A pair of braces  $\{\}$  creates an empty dictionary. Placing a comma-separated list of key-value pairs within the braces adds initial key-value pairs to the dictionary [Beazley 2006]. The dictionary example with the graph in Figure 3 is presented in (2).

### 4.3 Local minima

Stalactite extremities correspond to local minima in the 3D-mesh. A local minimum in the 3D-mesh surface is one point  $P$  of the mesh such that its  $z$  coordinate is less than  $z$  coordinates of all points in a chosen neighborhood of  $P$ .

A local minimum  $P$  is a vertex of the 3D-mesh because the faces of this surface are triangles. Thus, given a vertex  $v \in V$  to decide if it corresponding point on the 3D-mesh is local minimum it is sufficient to check if its  $z$ -coordinate is less than the  $z$ -coordinates of all adjacent vertices of  $v$ .

```

Data:  $G = (V, E)$ 
initialization;
 $L_m \leftarrow$  empty list;
for  $v \in V$  do
     $N(v) \leftarrow$  list of adjacent vertices to  $v$ ;
    if  $z_v \leq z_{v_i}$  for all  $v_i \in N(v)$  then
        append  $v$  to  $L_m$ ;
    end
end

```

**Algorithm 1:** Local minimum algorithm.

Regarding the fact that if  $u$  is adjacent to  $v$  and  $z_u < z_v$  than  $v$  is not a local minimum, Algorithm 1 can be implemented without need to check the minimum condition for all vertices of  $V$ .

The vertices adjacency and the identification of local minima have opened a vast field of study.

Figure 4 present a plane view with computed local minimum of the chamber. The 3D-mesh model obtained for a octree depth of 11 was used (see Table 3). These points was colored according the intensity values to attempt correlating or recognizing patterns.

This map allows the investigation of possibly stalactites distribution, alignment, and other properties of interest to the SIPCLIP project.

The same figure also shows distributions and localizations of the stations.

Besides local minima, other important layer is present in the Figure 4: the water collection bottles. These bottles were placed inside the cave chamber at strategic locations to collect water from stalactites drip water. The objective was to search possible correlations between quantity of water collected and existing stalactites. This work is in progress.

Other important case study from the 3D-mesh, evolving the graph was the extraction of *contour lines*. Contour lines, also known as contours, are lines that join all points of equal elevation ( $z$ -coordinate). Contours are used to denote elevation and depth.

<sup>3</sup><http://www.python.org/>

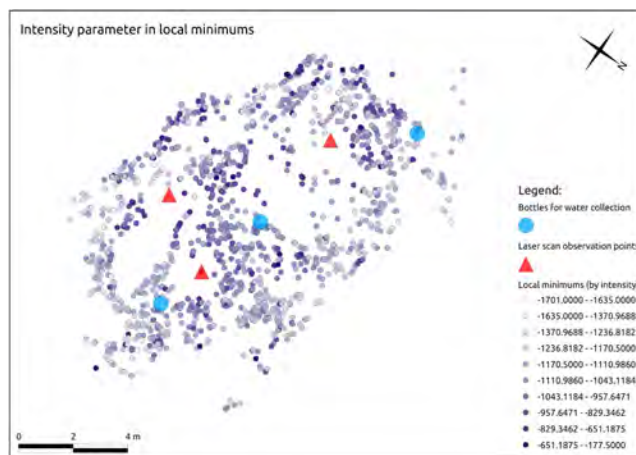


**Figure 4:** Plane view with local minima representing lower tip of stalactites.

In the context of the present work, contours allow denoting topographic surface of the chamber and are useful structures for water run-off studies. Figure 5 shows 5cm equidistant contours of a specific region of stalactites in the interior of Algar do Penico chamber.

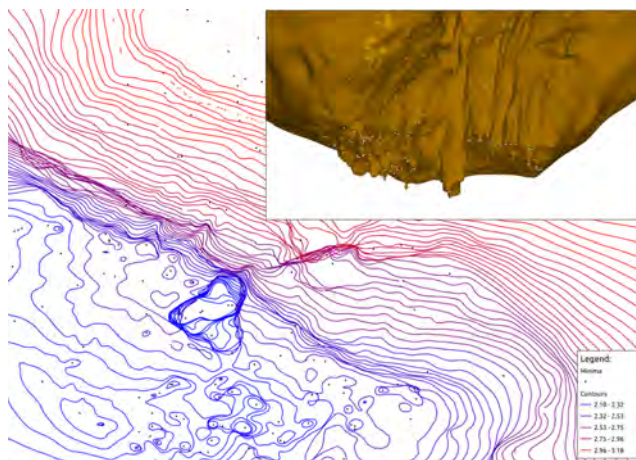


**Figure 5:** Plane view of contour lines and respective 3D-mesh showing stalactites.

## 5 3D data visualization on the Web

As a consequence of advances in computer hardware and Internet connection speed, Web3D sites that include three-dimensional models where users navigate and interact through a 3D graphical interface, are increasingly employed in different domains. The possibility to publish 3D data on the Web is of particular interest for the geospatial field. This enables researchers to visualize, navigate and interact with three-dimensional data on a simple Web browser [Costa et al. 2011]. In addition to the 3D-mesh publishing, we want to map geomorphological structures of the cave interior.

Several technologies exist to create 3D content for the web. Some of them are plug-in based systems, that means they depend on an additional piece of software running inside a web browser. These technologies have some clear disadvantages such as, the distrust, security and incompatibility issues associated with the plug-in installation and the need to understand how the plug-in works to de-

velop applications.

Nowadays, it is possible to integrate 3D content on the Web directly into the browser without plug-ins or additional components. This is the approach for the proposed framework presented in this paper that uses X3D, WebGL and X3DOM enabling the 3D visualization and navigation in the interior of the Algar do Penico in the Firefox, Google Chrome, Safari and Opera web browsers without specific plug-ins. X3D is used to represent the cave chamber 3D model and it is inserted on the user side for visualization in WebGL supported browsers with the X3D Document Object Model (X3DOM) technique. X3D is the ISO standard XML-based file format for representing 3D computer graphics. It is the successor of VRML, including a large number of new and extended features. A major difference between X3D and VRML is the use of XML as syntax. X3D benefits in many ways of using XML since it is easy to read for both humans and computer systems, it is well supported, it is license free, the data is well structured and it is web compatible [Cerbo et al. 2010].

WebGL is an open standard software library for a low-level 3D graphics API based on OpenGL that generates interactive 2D and 3D graphics on any browser without installing additional plug-ins. WebGL uses HTML5 to include data content into the DOM (Document Object Model) and access to this content in the scene graph but HTML5 cannot do this directly with 3D data. In this context, the Web3D consortium has written recommendations about how to integrate HTML5 and 3D content, more specifically, Extensible 3D (X3D) [Mao 2011]. Although X3D content is not supported by all web browsers directly right now, it is the trend that in the near future X3D elements will be able to be directly manipulated by the most common browsers with the DOM technique [Behr et al. 2009] [Prieto et al. 2012].

X3DOM is an open source framework with the objective of integrating HTML5 and X3D on top of WebGL [Behr et al. 2009]. X3DOM is a framework for integrating and manipulating (X3D) scenes as HTML5-DOM elements, which are rendered via WebGL and therefore does not require plug-ins for displaying the X3D content.

The 3D-mesh size is a problem for visualization efficiency and interactivity in real time on the Web. Models can present huge number of elements stored in large file size. Detailed and high-precision model can have 2.4GB. To produce a lighter model we decided to simplify the cave chamber 3D-mesh. One of the significant ways to simplify meshes is by geometry removal operations. These operations are called *mesh decimation* and consist in iteratively remove geometry unit such as vertices, edges or triangle faces [Heckbert and Garland 1999].

For the 3D-mesh simplification we used the MeshLab multi-edge decimation function called *Quadratic Edge Collapse Decimation*. This function consists in removing the multi-edge mesh and the relative triangles and then connect the adjacent vertices to the new vertex [Chen et al. 2007].

In order to select a 3D-mesh with a reasonable size that do not compromise performance for Web publishing we tried to simplify the generated 3D-meshes presented in Table 3 (Section 3). The Quadratic Edge Collapse Decimation worked with the 3D-meshes generated from 10 and 11 octree depth. The 11 octree depth 3D-mesh was chosen due to its higher detail level, which refers to higher number and dimension of stalactite.

Three simplifications were generated from the 11 octree depth 3D-mesh. Table 4 presents the number of vertices, the number of triangle faces and the size of each simplified 3D-mesh files in X3D format. These new simplified meshes were integrated with HTML5

using the *InstantReality*<sup>4</sup> framework. This framework provides tools for 3D data sets optimization. Tests of download time were performed in localhost environment. Waiting time varying between 7s and 60s were measured.

**Table 4:** Tests of download speed between three different mesh sizes.

# vertices	# faces	size (MB)	download time (s)
500732	998856	60.2	60
250791	499486	29.8	19
125497	249696	14.6	7

Considering the download times we selected the 3D-mesh with about 250 thousand faces and about 125 thousand vertices, as presented in Table 4. This 3D-mesh takes about 7 seconds to be ready for real time interaction in a Web browser.

Figure 6 illustrates the cave chamber 3D-mesh and its stalactites extremities represented by white dots. Lower tip of stalactites or local minima resulted from the algorithm 1 (Section 4.3). The same local minima are represented in Figure 4.

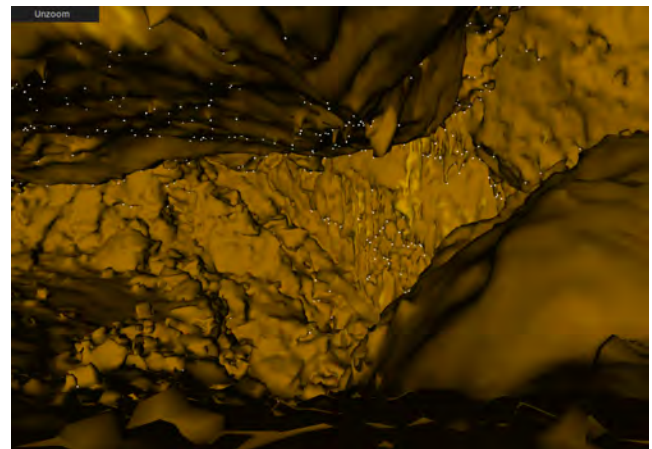


**Figure 6:** Web visualization of cave chamber 3D-mesh and local minima (stalactites extremities).

Figure 7 represents a 3D Web visualization of a particular area of interest. This area correspond to the biggest stalactite in the chamber. This visualization also contains the contour lines calculated for the same area.

The developed framework for 3D visualization of the cave chamber is available on the Web at the address: <http://193.136.227.170/sipclip/web3d/>.

## 6 Conclusion

This paper presented an approach for the 3D modeling and Web visualization of 3D data from a cave chamber. It was described a process of surveying with Terrestrial Laser Scanning technique. This was a complex task. Chambers have many irregular surfaces and we obtained a point cloud with about 45 million points with high level of detail. Using the intensity values of the point cloud we also showed that the coordinates of the scan points reveal a very high-precision of less or equal to 1mm.

<sup>4</sup><http://www.instantreality.org/>

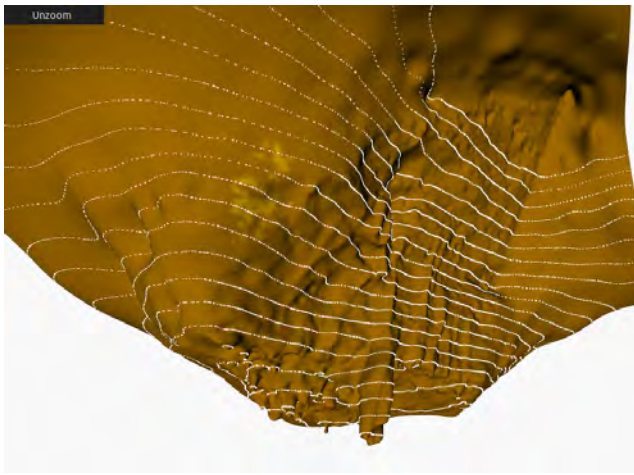


**Figure 7:** Web visualization of stalactite 3D-mesh and its contour lines.

It was a challenge to work with such massive data collection to generate a surface model of the cave chamber to study its geomorphological features. For the 3D modeling process we used an open source tool called MeshLab. This software allowed to generate a 3D-mesh from the original point cloud with the goal to achieve a compromise between the complexity of the 3D-mesh, the realistic visualization and real time interaction in the chamber 3D model. For this purpose, we used the Poisson Surface Reconstruction method that generated a 3D-mesh with a about 5 million vertices and 10 million faces.

One of the main goals of this research project was to visualize and identify cave stalactites that could provide information on hidden cave features responsible for cave geomorphology. Stalactites extremities are local minima in the 3D-mesh. We described in this paper an algorithm to find local minima for the recognition of stalactites distribution, alignments and other properties of interest to the SIPCLIP project. It is also presented a topological structure for the 3D-mesh to get an efficient algorithm for the process of finding stalactites structures.

A framework for 3D visualization of cave chamber was made available on the Web using X3D, WebGL and X3DOM. Such solution does not require any additional plug-ins. The availability of Algar do Penico in a Web3D is interesting for the geospatial field. Researcher can navigate in this environment to visualize stalactites extremities and contour lines.

## Acknowledgments

This work has been supported by the Portuguese government and EU - Funding, through the FCT - Fundação para a Ciência e Tecnologia funding of the SIPCLIP project (PTDC/AAC-CLI/100916/2008).

## References

BARBARELLA, M., AND FIANI, M. 2012. Landslide monitoring using terrestrial laser scanner: Georeferencing and canopy filtering issues in a case study. *ISPRS - International Archives of the Photogrammetry, Remote Sensing and Spatial Information Sciences XXXIX-B5*, 157–162.

- BEAZLEY, D. 2006. *Python: Essential Reference*. Developer's Library. Centraal Boekhuis.
- BEHR, J., ESCHLER, P., JUNG, Y., AND ZÖLLNER, M. 2009. X3dom: a dom-based html5/x3d integration model. In *Web3D*, ACM, S. Spencer, D. Fellner, J. Behr, and K. Walczak, Eds., 127–135.
- BERNARDINI, F., MITTLEMAN, J., RUSHMEIER, H. E., SILVA, C., AND TAUBIN, G. 1999. The ball-pivoting algorithm for surface reconstruction. *IEEE Trans. Vis. Comput. Graph.* 5, 4, 349–359.
- CERBO, F. D., DODERO, G., AND PAPALEO, L. 2010. Developing a web 3.0 e-learning portal with x3d technologies. In *Eurographics Italian Chapter Conference*, 129–134.
- CHALMOVIANSKY, P., AND JUTTNER, B. 2003. Filling holes in point clouds. In *Mathematics of Surfaces, Proceedings of the 10th IMA International Conference*, Springer, M. J. Wilson and R. R. Martin, Eds., vol. 2768 of *Lecture Notes in Computer Science*.
- CHEN, H., LUO, X., AND LING, R. 2007. Surface simplification using multi-edge mesh collapse. In *Image and Graphics, 2007. ICIG 2007. Fourth International Conference on*, 954–959.
- CIGNONI, P., CALLIERI, M., CORSINI, M., DELLEPIANE, M., GANOVELLI, F., AND RANZUGLIA, G. 2008. Meshlab: an open-source mesh processing tool. In *Eurographics Italian Chapter Conference*, Eurographics, V. Scarano, R. D. Chiara, and U. Erra, Eds., 129–136.
- COSTA, C., RODRIGUES, J., AND FIGUEIREDO, M. 2011. A web3dgis framework using citygml and x3d. In *Proc. of 5th Ibero-American Symposium in Computer Graphics*, 113–116.
- FORD, D. C., AND WILLIAMS, P. 2007. *Karst Hydrogeology and Geomorphology*. Wiley.
- GLASSNER, A. 1994. Building vertex normals from an unstructured polygon list. In *Graphics Gems IV*, P. Heckbert, Ed. Academic Press Professional, Inc., San Diego, CA, USA, 60–73.
- HECKBERT, P. S., AND GARLAND, M. 1999. Optimal triangulation and quadric-based surface simplification. *Computational Geometry* 14, 1–3, 49–65.
- KAZHDAN, M. M., BOLITHO, M., AND HOPPE, H. 2006. Poisson surface reconstruction. In *Symposium on Geometry Processing*, Eurographics Association, A. Sheffer and K. Polthier, Eds., vol. 256 of *ACM International Conference Proceeding Series*, 61–70.
- PRIETO, I., IZKARA, J., AND DELGADO, F. 2012. From point cloud to web 3d through citygml. In *Virtual Systems and Multimedia (VSM), 2012 18th International Conference on*, 405–412.
- RONCAT, A., DUBLYANSKY, Y., SPOTL, C., AND DORNINGER, P. 2011. Full-3d surveying of caves: A case study of marchenhöhle (austria). In *Proceedings of the International Association for Mathematical Geosciences (IAMG 2011)*.
- SHEN, C., O'BRIEN, J. F., AND SHEWCHUK, J. R. 2004. Interpolating and approximating implicit surfaces from polygon soup. *ACM Trans. Graph.* 23, 3, 896–904.
- SILVESTRE, I., RODRIGUES, J., FIGUEIREDO, M., AND VEIGAPARES, C. 2012. Modelação 3d de grutas. In *Proc. of 6th International Conference on Digital Arts*, 461–464.

- TOBLER, R., AND MAIERHOFER, S. 2006. A mesh data structure for rendering and subdivision. In *International Conference in Central Europe on Computer Graphics, Visualization and Computer Vision*, 157–162.
- TSAKIRI, M., SIGIZIS, K., BILLIRIS, H., AND DOGOURIS, S. 2007. 3d laser scanning for the documentation of cave environments. In *11th ACUUS Conference: Underground Space: Expanding the Frontiers*.
- VOEGTLE, T., SCHWAB, I., AND LANDES, T. 2008. Influences of different materials on the measurements of a terrestrial laser scanner (tls). In *ISPRS - International Archives of the Photogrammetry, Remote Sensing and Spatial Information Sciences*, vol. XXXVII-B5, 1061–1066.